[14] Retroperitoneal space organ segmentation from CT images based on the level set function

R.V. Eruslanov[1], M.N. Orehova[1], V.N. Dubrovin[2]
[1]Volga State University of Technology, Yoshkar-Ola, Russia
[2]Republican Clinical Hospital of the Mary-El Republic, Yoshkar-Ola, Russia

Abstract

This article presents the method of solving the problem of segmentation of the retroperitoneal space organs from the tomographic images; the method bases on the level set function. The method of image pre-processing is based on the nonlinear anisotropic diffusion filter which smooths the image while maintaining the edges between the segments. The segmentation algorithm of tomographic image based on the level set function are synthesized.

Keywords: *segmentation, computer tomography, retroperitoneal space organs, CT, image processing, anisotropic diffusion, nonlinear filtration, level set, active contour.*

Citation: *Eruslanov R.V. Retroperitoneal space organ segmentation from CT images based on the level set function / Eruslanov R.V., Orehova M.N., Dubrovin V.N. // Computer Optics. – 2015. – Vol. 39(4). – P. 592-599*

Introduction

3D simulations technology of computed tomography (CT) data are more actively used by doctors in their medical practice, significantly increasing the information content of studies [1-4], facilitating the identification of pathologies or optimizing preoperative planning [5, 6] However, for some clinical problems such as surgical preoperative planning [5, 6, 9, 10], it is necessary to understand the three-dimensional data structure, which is quite challenging and in many respects depends on the physician's experience. Image segmentation is a necessary image processing step for solving such problems [5, 7, 8]. Segmented 3D visualization of human organs gridded to the patient makes it much easier to understand images and speeds up the learning process for novice surgeons. 3D representation of segmented models of human organs is an integral part of all surgical simulators [7, 11-13], which simulate surgical steps on virtual models.

The paper deals with application of level functions for numerical simulation of the patient's organs image segmentation process based on the results of the tomographic examination. Segmentation process depends on many factors, such as curvature of segmented regions, the intensity distribution or image structure. Methods based on the level function are characterized by adaptability to the parameters of the original image, which reduces the complexity of managing the process of segmentation of medical images.

Objective: Development of an algorithm of segmentation of images of human organs on CT images based on the level function.

1. Theoretical analysis

With reference to the tomography image segmentation task is understood as the task of division of digital image into a plurality of disjoint regions or pixels sets, having the same sign characteristic, e.g., texture, color or intensity, depending on the type of tissue and anatomic structure. Adjacent areas differ from each other by the same characteristics. The result of segmentation is a set of areas covering the entire image, and a set of contours extracted from them.

To date, the problem of segmentation is generally considered to be unsolved, because there is no clear and unambiguous formulation of the general problem. The working result of the methods based on machine learning [14, 15], fairly depend on the characteristics of the training set. Methods based on a priori models [16, 17] and probabilistic atlases [18, 19], also have a number of problems, because they require

time-consuming operations in the preliminary stage of formation models: collection and classification of samples and manual segmentation. These methods in most cases are highly efficient and simple, but at the same time, give inadequate results in the processing of non-standard images, or have a high computational cost. Methods based on active contours and level functions are more universal and have no such problems. Lefohn et al. [20] and Cates et al. [21] showed that the segmentation techniques based on the level function reduce complexity of the segmentation process of medical images. The main difficulty in their development is the synthesis of adequate speed function and its parameters.

Suppose the original image is represented as a four-dimensional scalar (x, y, z, i) field, where x, y, z are the coordinates of pixels, and i is intensity value. Then as the level function $\phi(\mathbf{u}): \Re^4 \to \Re$, $\mathbf{u} = (x, y, z)$ of the image a mathematical object ϕ is understood, implicitly representing the image Ω_1 and outside Ω_2 areas (Figure 1). Ω_1 field corresponds to the highlighted segment, and Ω_2 – to other segments or background. $\phi(\mathbf{u})$ function is given by a scalar field, which takes positive values for Ω_1 region and negative for Ω_2:

$$\Omega_1 = \{\mathbf{u} : \phi(\mathbf{u}) \geq 0\} \text{ and } \Omega_2 = \{\mathbf{u} : \phi(\mathbf{u}) < 0\}, \quad (1)$$

where $\mathbf{u} = (x, y, z)$ is the coordinate of the image pixel.

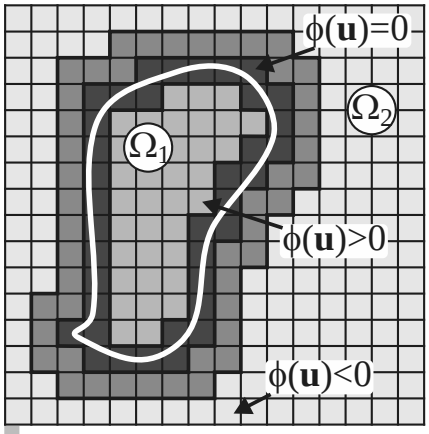

Fig.1. To determine the function level

If the number of segmented regions $N > 2$, then N functions are used of the level $\{\phi_h\}_{h=1}^{N}$, which divide image on the regions $\{\Omega_h\}_{h=1}^{N}$. Contours B_h of segments are defined by points lying on the regions` border $\{\Omega_h\}_{h=1}^{N}$, i.e.:

$$B_h = \{\mathbf{u} : \phi_h(\mathbf{u}) = 0\} \quad (2)$$

Level ϕ_h function is initiated by 3D region V_h^0 (also called bare area or "grain") within a 3 D image:

$$\phi_h(\mathbf{u}) = 1, \ \forall \mathbf{u} : \mathbf{u} \in V_h^0, \ \ \phi_h(\mathbf{u}) = -1, \ \forall \mathbf{u} : \mathbf{u} \notin V_h^0 \quad (3)$$

The surface feature ϕ is iteratively deformed so as to highlight the image region of interest. Wherein the function ϕ motion takes place along the normal

$$N = -\frac{\nabla\phi(\mathbf{u})}{|\nabla\phi(\mathbf{u})|}$$

to the function surface ϕ at the $\mathbf{u}$ point. The speed of the evolutionary process of the function ϕ is governed by locally dependent function of the speed $F(\mathbf{u}, t)$:

$$\phi(\mathbf{u}, t + \Delta t) = \phi(\mathbf{u}, t) + \Delta t \cdot F(\mathbf{u}, t) \cdot |\nabla\phi(\mathbf{u}, t)| \quad (4)$$

where $\mathbf{u}$ is the pixel coordinate, t is current time of segmentation process, Δt – discretization by time, $\phi(\mathbf{u}, t)$ and $\phi(\mathbf{u}, t + \Delta t)$ are values of the level function of the last and the next iteration. A more complete overview of the methods based on the level function and their application to image segmentation can be found in Sethain [22], Osher and Paragios [23].

2. The mathematical model of image

We used the data of the standard clinical examination of spiral computed tomography performed on devices Philips Brilliance 64 Siemens Somatom 40, in cooperation with the Republican Clinical Hospital of Mari El. Images are stored in the DICOM format.

CT image I is an ordered set $I = \{I_z\}_{z=0}^{N-1}$, from N x-ray images of the human body, made at a definite distance $K = \{k_x, k_y, k_z\}$ between pixels. Each pixel $\mathbf{u} = (x, y, z)$ of such image is encoded by the shifted value of the quantifying estimation of the density $I(\mathbf{u})$ of human tissue structures on the scale of Hounsfield. Range scale units range from -1024 to +3071, pixel intensity value lies in the range $0 \leq I(\mathbf{u}) \leq 4095$. The range is rather wide and allows to classify certain tissues confidently [8].

Images of retroperitoneal organs on CT images obtained as the result of examination have inconsistent intensity. This is due to the heterogeneity of tissue and organs structure, most tissues contain blood, which leads to the "noisy" images. An element of randomness is also laid in the very nature of the radiation source. Thus, the mathematical model of the CT image I is as follows:

$$I = b \cdot J + Z \quad (5)$$

where J is undistorted("perfect") image, b is a component asssosiated with image heterogeneity, Z is additive noise, I is the resulting image issued by tomograph. We assume that within a single tissue component b varies monotonically and smoothly, and the noise component Z is subject to the normal distribution law.

3. Pre– processing of image

The section discusses the method of pre-processing of images, reducing the influence of the noise components b и Z (5), and approximating the result of processing

to the «ideal» image J, at the same time preserving boundaries between the segment areas.

Traditional methods of removing noise, improving margins and reconstruction of blurred images are based on high-frequency filtering methods, or reverse spread of the diffusion equation in time. The problem in the current setting can be solved, using as a physical basis a non-linear process of diffusion. P. Perona and J. Malik [24] reported that, if the conductivity coefficient is selected in accordance with the gradient function of the image, the diffusion will simultaneously smooth the image and enhance the edges, stabilizing the image to echelon form. The result is guaranteed by the principle of maximum diffusion equation.

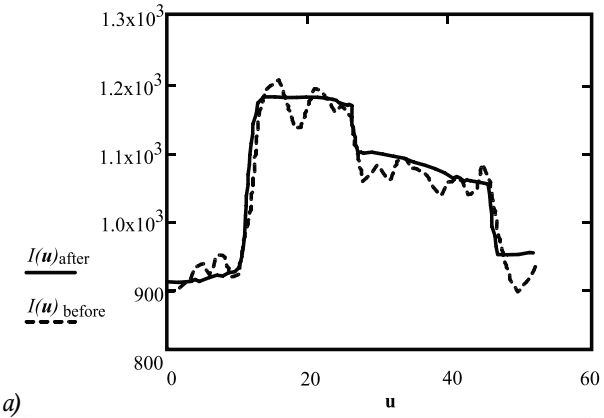

a)

b)

Fig.2. Work of anisotropic diffusion filter: a) for a one-dimensional slice (by solid line the original image is indicated, by the dotted line – the filtered one); b) for one 2D slice, the intensity is plotted along the axis OZ, top picture is the original fragment of image, the bottom is the image after filtering

Anisotropic diffusion filter works as follows. To the filter input are sent I of tomograms slices, scale coefficients $K = \{k_x, k_y, k_z\}$ CT images, which describe physical distance between the pixels, and taken into account when calculating the gradient $\nabla I(\mathbf{u})$. Then iteratively to each pixel is assigned a new intensity value according to the formula:

$$I'(\mathbf{u}) = I(\mathbf{u}) + \Delta I(\mathbf{u}) = \\ = I(\mathbf{u}) + \nu \cdot div\left(\nabla I(\mathbf{u}) \cdot \exp\left(-\frac{|\nabla I(\mathbf{u})|}{\kappa^2}\right)\right). \quad (6)$$

If diffusion $\Delta I(\mathbf{u})$ in a fixed neighborhood of a point $\mathbf{u}$ is large, then this intensity at that point is the noise and the intensity value is adjusted toward the dominant intensity. If diffusion $\Delta I(\mathbf{u})$ is small, then the point belongs to the boundary and no blurring occurs. A more detailed description of the mechanism of filter performance can be found in the article P. Perona and J. Malik [24]. Among the advantages of the filter should be noted stability and parallelizability.

The gradient $\nabla I(\mathbf{u})$ is estimated for $3\times3\times3$ of point neighborhood. The number of iterations steps is equal to 16 [24]. Selection of ν parameter, responsible for smoothness of the diffusion process, is discussed in the article G. Gerig et al. [25]. In this paper, the value $\nu = 0{,}142857$. Parameter κ performs the same role as the mean-square deviation in the model of the normal distribution law and influences the process of smoothing. The higher the parameter κ value, the greater range of intensities is exposed to smoothing. A working range of parameter values for CT images of retroperitoneal organs is experimentally set: $\kappa \approx 25 \pm 5$.

Figure 2 shows the working result of the anisotropic diffusion filter.

4. The detector function of boundaries

As in the previous step an anisotropic diffusion filter is used which minimizes the spread of values in the uniform area, but maintains the border, in the role of the border detector function a function type may be used:

$$g(\mathbf{u}) = \frac{1}{1+\sigma^2[I(\mathbf{u})]}, \quad (7)$$

where $\sigma^2[I(\mathbf{u})]$ is dispersion of brightness values in the radius range $r = 1{,}5$ pixels around the point $\mathbf{u}$. This type of function detects the borders with sufficient sensitivity to weak brightness drops. Fig. 3b shows the working result of the function of borders detector (7). It is worth paying attention to the frag-

ment of the CT image, comprising transition from liver to muscles (Fig. 3, is marked by the square). As can be seen from Figure 3b, the detector detects this border.

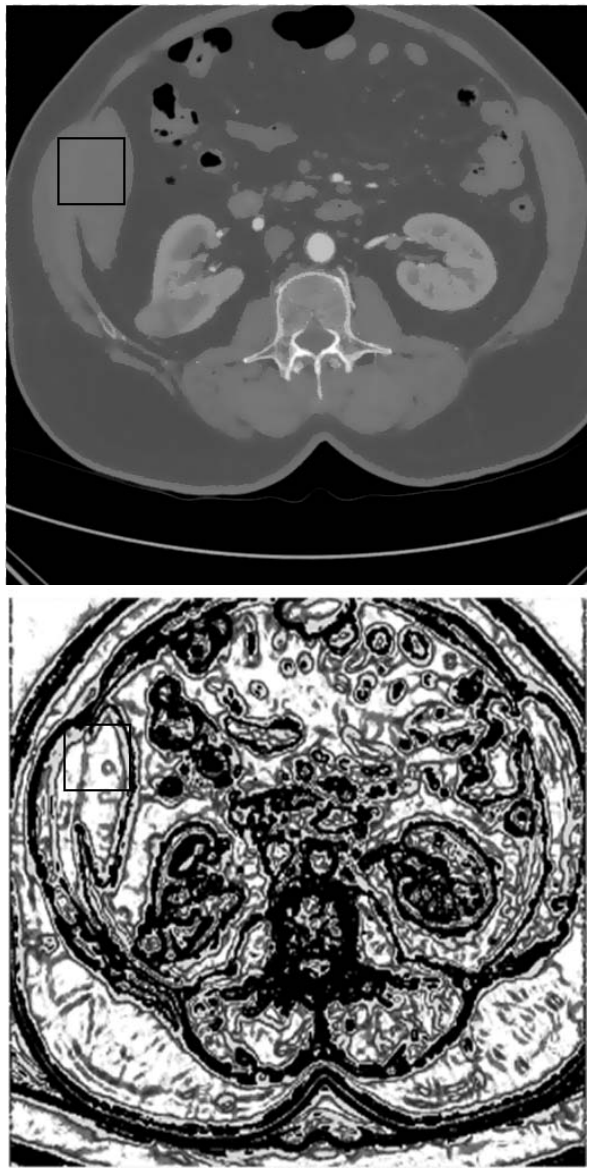

Figure 3. Result of work of the boundaries detector function g (u): a) CT image after applying the anisotropic diffusion filter; b) display of the values of the function g (u), the white areas correspond to homogeneous image areas, black areas – to the boundary regions between the segments

5. The functional of the level function

To manage the evolution of the level function (4) a locally dependent speed function is used $F(\mathbf{u},t)$. The function evaluates the speed of evolution according to the local surface curvature of the level function $\phi(\mathbf{u},t)$ and the local intensity of image I.

There are two requirements to the speed function. First, functions $\phi(\mathbf{u},t)$ must vary along the normal to its surface. Second, the evolution of the function $\phi(\mathbf{u},t)$ must be decelerated on reaching segment boundaries.

Speed function for the function of the level ϕ_h is built under the scheme with smoothing [26]:

$$F_h(\mathbf{u},t) = \alpha \cdot C_h(\mathbf{u},t) + (1-\alpha) \cdot D_h(\mathbf{u}) \quad (8)$$

where $\alpha \in [0,1]$ is the smoothing function which controls the relative influence of the curvature values $C_h(\mathbf{u},t)$ and information term $D_h(\mathbf{u})$ at the behavior of the speed function, h is the number of level function. The α parameter value can be associated with the function of the boundaries detector: $\alpha = g(\mathbf{u})$ (7). This technique allows the circuit to switch smoothly between modes of propagation along the normal to the function for a homogeneous area ($g(\mathbf{u}) > 0$) and distribution near the boundary between the segments ($g(\mathbf{u}) \approx 0$).

Informational term $D_h(\mathbf{u})$ is responsible for the sign and power of the speed function for h function of the level and is defined as follows:

$$D_h(\mathbf{u}) = \varepsilon_h - |I(\mathbf{u}) - T_h| \quad (9)$$

where $I(\mathbf{u})$ is the function of the image intensity, T_h is the target intensity which stimulates the maximum surface growth, and ε_h is the intensity range in which the level function must grow. If the value of intensity $I(\mathbf{u})$ at the $\mathbf{u}$ point satisfies the condition $T_h - \varepsilon_h \le I(\mathbf{u}) \le T_h + \varepsilon_h$, then $D_h(\mathbf{u})$ promotes the growth (expansion) of the region, or otherwise – compression of the area.

The intensity distribution of the biological tissue is random. Experimental test on a group of patients showed that the intensity distribution of individual structural elements of organs and tissues within the image of one patient corresponds to the normal distribution law with a confidence level of 0.95 (Kolmogorov test). Therefore the quantitative estimations of T_h and ε_h parameters can be set by mathematical expectation μ_h and an average quadratic deviation σ_h for each level feature:

$$T_h = \mu_h = M[I(\mathbf{u})],\ \varepsilon_h = k \cdot \sigma_h = k \cdot \sigma[I(\mathbf{u})],\ \mathbf{u} \in \phi^h \quad (10)$$

where k is a parameter chosen, e.g., by the rule of "three sigmas", $k = 3$.

Parameters T_h and ε_h change iteratively in the process of evolution of each function of the level. The initial values of the parameters are measured at the intensity values of a set of initiating seed field points V_h^0.

The curvature of the level function at the point $\mathbf{u}$ is defined as a local divergence of the normalized gradient of function of the level at the previous iteration:

$$C_h(\mathbf{u},t) = div \frac{\nabla \phi_h(\mathbf{u}.t - \Delta t)}{|\nabla \phi_h(\mathbf{u}.t - \Delta t)|} \quad (11)$$

The gradient ∇ is calculated for the $3 \times 3 \times 3$ pixel area according to the scheme presented in [26]. This area of connectivity gives a smoother surface curvature assessment of level function.

In the role of initial seed regions V_h^0 are used 3D spherical fragments of the radius image $\rho = 3$ of a pixel with centers in points $\mathbf{u}_h^0$, arranged in nodes of regular grid.

Since the points falling within the sphere window are used to estimate the initial statistics T_h и ε_h, then for their correct estimation the centers $\mathbf{u}_h^0$ must lie within the segmented region and should not be at the border of two segments. If seed area is on the border of segments, the intensity distribution is characterized by a high level of dispersion owing to the presence of several centers of mass. Therefore, a criterion for dropping out of such areas can be the use of condition for standard deviation with a threshold, for example, $\varepsilon_h > 20$.

In the process of evolution a situation is inevitable where two level functions will be in contact by their borders. In this case quantitative values are measured of the degree of similarity of the pixel intensity values for each of the competing segments Ω_h using the likelihood function:

$$L_h(\mathbf{u}) = \frac{1}{\sigma_h\sqrt{2\pi}}\exp\left(-\frac{(I(\mathbf{u})-\mu_h)^2}{2\sigma_h^2}\right). \quad (12)$$

And by the criterion of maximum likelihood a pixel will relate to one of the adjacent segments

At each step of the segmentation process statistics is kept of the evolution of level functions in the form of *Count* of added/ excluded points.

$$Count = \sum_{\mathbf{u}\in I}\begin{cases}0, & \phi(\mathbf{u},t) = \phi(\mathbf{u},t+\Delta t)\\ 1, & \phi(\mathbf{u},t) \neq \phi(\mathbf{u},t+\Delta t)\end{cases} \quad (13)$$

The evolution process goes on until the functions of the level stabilize, their growth stops, and *Count* becomes less than a certain threshold value $Count_{threshold}$.

At the last step there is a fusion of adjacent functions of the level having common statistics, e.g. at the Kolmogorov-Smirnov criterion [27].

Thus, the proposed generalized image segmentation algorithm based on function of the level is as follows:

1. Application of anisotropic diffusion filter for each point $\mathbf{u} \in I$ according to equation (6).
2. Calculation of function of borders detector $g(\mathbf{u})$ for the neighborhood of the radius $r = 1{,}5$ pixels of each point $\mathbf{u}$ according to equation (7).
3. Generation of a plurality of seed regions $\{V_h^0\}_{h=1}^N$ and initialization of level functions $\{\phi_h\}_{h=1}^N$ according to equations (3) and (10).
4. Iterative change of the level function according to equations (4) and (8) until stabilization.
5. Visualization of results.

This algorithm is implemented under the scheme with parallel computing. Thus in steps 1 and 2, there is no need to synchronize the interaction of simultaneously carried out threads. While steps 3 and 4 during their work require a mechanism of synchronization and control of mutually exclusive access to shared resources.

6. The results and further work

The algorithm has been implemented as a part of "Volga-M" software, developed at the Department of radio engineering and biomedical systems, in collaboration with the urology department of the Republican Clinical Hospital of Mari El. Job was tested on CT data of three patients with urological pathologies. The result of algorithm operation with a single grain on one of the images of kidney and tumor is shown in Figure 4.

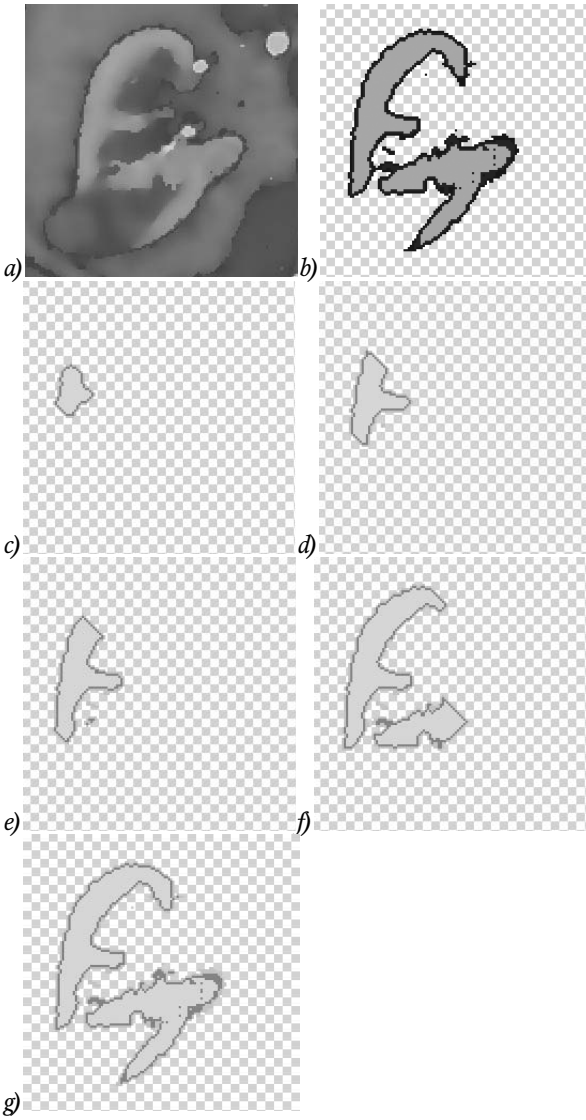

Figure 4. Stepwise evolution of level function for one seed: a) the original kidney image, b) a segmentation result of kidney cortex, c) to g) view of the level of function at 10, 20, 30, 50, and 70 iterations, respectively,

In general, the algorithm runs stably and allows to segment individual classes and structure of the patient's organs. When segmenting a plurality of grains the segmented image of the patient body is formed. Figure 5 shows the evolution of functions of the level in this image segmentation mode. Expertise in the face of the medical practitioner has shown that the basic structure of the kidneys are allocated correctly.

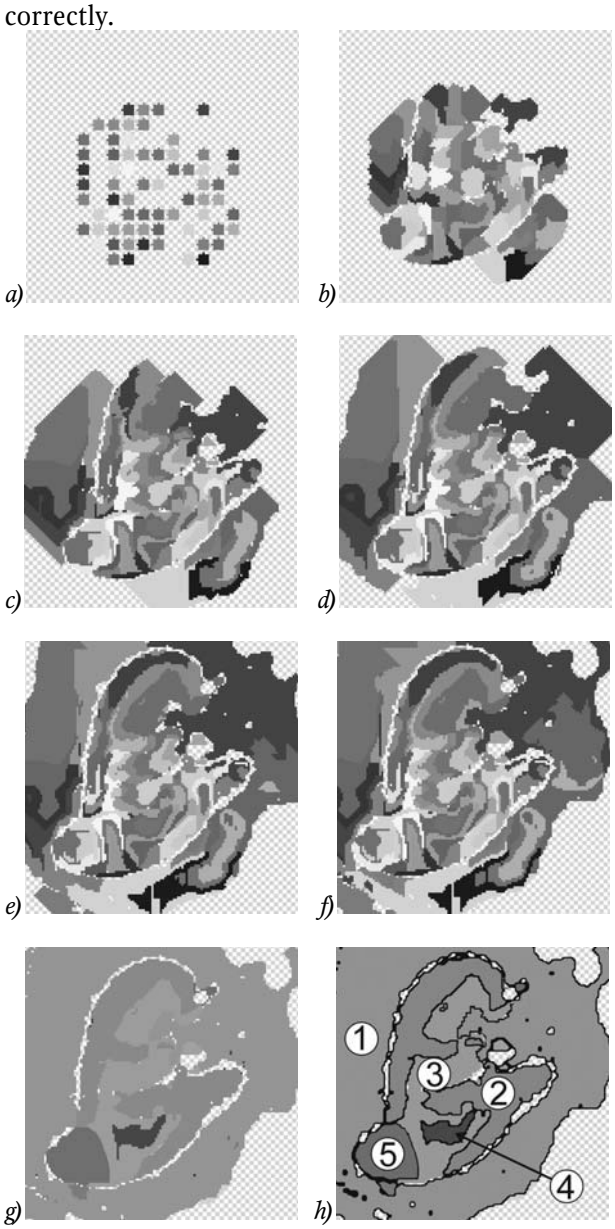

Figure 5. Stepwise evolution of level function for multiple seed: a) the type of the original set of seed, b) to f) view of the level functions for 10, 30, 50, 70, 90 iterations, respectively, g) -h) segmentation result at 90 iterations after association of related functions of the level: the surrounding tissue (1), kidney cortex (2), the kidney parenchyma (3, 4), tumor (5)

The disadvantage of the current implementation of the algorithm may include not quite effective using the results obtained at a stage of selection of boundaries. Potentially, a combination of anisotropic diffusion filter and boundaries detector function detects the boundaries between segments with smoothly changing brightness characteristics. Implementation of the scheme of evolution of level function in conjunction with the methods of morphological processing of the result of boundaries detector function may allow to form more rigorous evolutionary terms. The further work on the project will be devoted to this area.

Conclusion

This paper proposes a method of segmentation of retroperitoneal space organs on the tomographic images based on the function of the level . To implement this method we inspected the mathematical model of the CT image, taking into account the statistical properties of the structural elements of organs and tissues and the effect of noise. On the basis of the constructed mathematical model a method is proposed for pre-processing the image based on the application of the nonlinear adaptive anisotropic diffusion filter which is smoothing the image while maintaining the boundaries between segments, and functions of the boundaries detector based on the dispersion estimation of values of a point surroundings. This approach to the pre-treatment image gets rid of the influence of the noise component, saves the information on the internal structure of tissues and organs by maintaining the boundaries between large isolated segments. A tomographic image segmentation algorithm was synthesized basing on the level function and active circuits, and examples of its operation are given. The developed algorithm can be used for engineering and medical practice in the development of medical imaging software, training simulation programs of preoperative planning and intraoperative navigation.

Acknowledgements

This work was made under the program UMNIK 2014, conducted by the Federal State Organization "Foundation for Assistance to Small Innovative Enterprises in Science and Technology" (a government contract number 4334GU1 / 2014, code 000790).

References

1. Blackmore CC, Mecklenburg RS, Kaplan GS. Effectiveness of clinical decision support in controlling inappropriate imaging. Journal of the American College of Radiology 2011; 8(1): 19-25.

2. Brouwer OR, Buckle T, Bunschoten A, Kuil J, Vahrmeijer AL, Wendler T, Valdes-Olmos RA, Van Der Poel HG, Van Leeuwen FWB. Image navigation as a means to expand the boundaries of fluorescence-guided surgery. Physics in Medicine and Biology 2012; 57(10): 3123-3136.

3. Rozhentsov AA, Doubrovin VN, Bayev AA, Naoumov AS. 3D image generation at prostata gland transurethral resection (in Russian). Vest. Povol. Gos. Tekhn. Univ. 2008; 3 : 45-50.

4. Su LM, Vagvolgyi BP, Agarwal R, Reiley CE, Taylor RH, Hager GD. Augmented reality during robot-assisted laparoscopic partial nephrectomy: toward real-time 3D – CT to stereoscopic video registration. Urology 2009; 73: 896-900.

5. Mitterberger M, Pinggera GM, Peschel R, Bartsch G, Pallwein L, Frauscher F. The use of three-dimensional computed tomography for assessing patients before laparoscopic adrenal-sparing surgery. BJU Int 2006; 98(5): 1068-1073.

6. Dubrovin VN, Bashirov VI, Eruslanov RV, Furman YA, Kudryavtsev AA. The first experience of computer optimization method of minimally invasive surgical approach based on preoperational tomographic data in performing retroperitoneoscopic ureterolithotomy (in Russian). Medical bulletin of Bashkortostan 2013; 8(3): 38-41.

7. Volonte F, Pugin F, Bucher P, Sugimoto M, Ratib O, Morel P. Augmented reality and image overlay navigation with OsiriX in laparoscopic and robotic surgery: Not only a matter of fashion. Journal of Hepato-Biliary-Pancreatic Sciences 2011; 18(4): 506-509.

8. Sharp G, Fritscher KD, Pekar V, Peroni M, Shusharina N, Veeraraghavan H, Yang J. Vision 20/20: Perspectives on automated image segmentation for radiotherapy. Medical Physics 2014; 41(5): DOI: 10.1118/1.4871620.

9. Emel'ianov SI, Veredchenko VA, Pushkar' DY, Mitichkin AE, Veredchenko AV, Shcherbakov NV. The use of intraoperative navigation in laparoscopic nephrectomy (in Russian). Endoscopic surgery 2009; 2: 32-35.

10. Huppertz A, Radmer S, Asbach P, Juran R, Schwenke C, Diederichs G, Hamm B, Sparmann M. Computed tomography for preoperative planning in minimal-invasive total hip arthroplasty: Radiation exposure and cost analysis. European Journal of Radiology 2011; 78(3): 406-413.

11. Dubrovin VN, Bashirov VI, , Furman YaA, Rozhentsov AA, Kudryavtsev AA., Eruslanov RV, Bayev AA, Nazarov IL. Hardware/software complex for selection optimal location for a trocar in laparoscopy (in Russian). Pat RF of Invent N127615 of August 15, 2012.

12. Dubrovin VN, Bashirov VI, Furman YA, Rozhentsov AA, Yeruslanov RV, Kudryavtsev AA. Choice of surgical access for retroperitoneoscopic ureterolithotomy according to the results of 3D reconstruction of operational zone agreed with the patient: initial experience. Central European Journal of Urology 2013; 66(4): 447-452.

13. Dubrovin VN, Bashirov VI, Furman YA, Rozhentsov AA, Eruslanov RV, Kudryavtsev AA. Optimization of computer-assisted surgical access during the retroperitoneal endoscopic ureterolithotomy using the patient coordinated 3D reconstruction of the operation area (in Russian). Experimental and Clinical Urology 2013; 4: 86-89.

14. Koss JE, Newman FD, Johnson TK, Kirch DL. Abdominal organ segmentation using texture transforms and a hopfield neural network. Correspondences of IEEE Transaction on Medical Imaging 1999; 18(7): 640–648.

15. Lee CC, Chung PC, Tsai HM. Identifying multiple abdominal organs from CT image series using a multimodule contextual neural network and spatial fuzzy rules. IEEE Transaction on Information Technology in Biomedicine 2003; 7: 208–217.

16. Soler L, Delingette H, Malandain G, Montagnat J, Ayache N, Koehl C, Dourthe O, Malassagne B, Smith M, Mutter D, Marescaux J. Fully automatic anatomical, pathological, and functional segmentation from CT scans for hepatic surgery. Computed Aided Surgery 2001; 6(3): 131–142.

17. Lamecker H, Lange T, Seebass M. Segmentation of the liver using a 3D statistical shape model. ZIBReport 04-09 (April 2004) 2004: 1–25. DOI:10.1.1.90.6969.

18. Park H, Bland P, Meyer C. Construction of an abdominal probabilistic atlas and its application in segmentation. IEEE Transactions on Medical Imaging 2003; 22(4): 483–492.

19. Zhou X, Kitagawa T, Hara T, Fujita H, Zhang X, Yokoyama R, Kondo H, Kanematsu M, Hoshi H. Constructing a Probabilistic Model for Automated Liver Region Segmentation Using Non-contrast X-Ray Torso CT images. Medical Image Computing and Computer-Assisted Intervention – MICCAI 2006.; 4191: 856-63.

20. Lefohn A, Cates JE, Whitaker RT. Interactive, GPU-based level sets for 3D segmentation. Medical Image Computing and Computer-Assisted Intervention – MICCAI 2003; 2878: 564–572.

21. Cates J, Lefohn A, Whitaker R. GIST: an interactive, GPU-based level set segmentation tool for 3D medical images. Medical Image Analysis 2004; 8(3): 217–231.

22. Sethain JA. Level Set Methods and Fast Marching Methods: Evolving Interfaces in Computational Geometry, Fluid Mechanics, Computer Vision, and Materials Science. Cambridge University Press; 1999.

23. Osher S, Paragois N. Geometric Level Set Methods in Imaging, Vision, and Graphics. Springer-Verlag New York,Inc.; 2003.

24. Perona P, Malik J. Scale space and edge detection using anisotropic diffusion. IEEE Transactions on Pattern Analysis and Machine Intelligence 1990; 12(7): 629-639.

25. Gerig G, Kikinis R, Kubler O, Jolesz FA. Nonlinear Anisotropic Filtering of MRI Data. IEEE Transactions on Medical Imaging 1992; 11(2): 221-232.

26. Lefohn AE, Kniss JM, Hansen CD, Whitaker RT. A streaming narrow-band algorithm: Interactive computation and visualization

of level sets. IEEE Trans. on Visualization and Computer Graphics 2004; 10(4): 422–433.

27. Lemeshko BY, Lemeshko SB, Postovalov SN, Chimitova EV. Statistical data analysis, simulation and study of probability regularities. Computer approach: monograph. (in Russian). – Novosibirsk : NSTU Publisher; 2011.